Optimization of a Molten Salt Electrolytic Bath Geometry for Rare Earth Metal Recovery using a Finite Element Method

Hiroo Numata[a], Hiroshi Akatsuka[b], and Haruaki Matsuura[b]

[a] Graduate School of Metallurgy and Ceramics Science, Tokyo Institute of Technology, 2-12-1-S8-7, Ookayama, Meguro-ku, Tokyo 1528552, Japan

[b] Research Laboratory for Nuclear Reactors, Tokyo Institute of Technology, 2-12-1-N1-10, Ookayama, Meguro-ku, Tokyo 1528550, Japan

Reprint requests to H. M. and H. N; E-mail: hmatsuur@nr.titech.ac.jp and numata.h.aa@m.titech.ac.jp

Z. Naturforsch. **68a,** 48 – 58 (2013) / DOI: 10.5560/ZNA.2012-0106
Received October 16, 2012 / published online February 15, 2013

For a recycling procedure for rare earths from spent hydrogen absorbing alloys by rare earths electrodeposition in a molten salt, the electrolytic bath and the cathode accessories have been optimized by evaluating the appropriate secondary current distribution using finite element method (FEM) computer simulation. The desirable cathode dish as an accessory was designed to prevent drops of less adherent electrodeposits, which improved the current density distribution compared with an a priori determined one. In the bath optimization, a reciprocal proportionality of the difference between the maximum and minimum current densities vs. the ratio of volume to surface area (or electrolyte volume) was found. It was found by FEM that if a resistive floating mass is assumed on the electrolyte surface, the observed necking in the electrodeposit near the electrolyte surface can be analyzed.

Key words: Computer Simulation; Finite Element Method; Secondary Current Distribution; Rare Earth; Molten Salt; Electrolytic Bath.

1. Introduction

The development of the molten salt industry has been rather slow, mainly because of the difficult handling of these substances and a lack of scientific and engineering data. Even though computer simulations are a promising tool, research and development work using these techniques has been especially rare in the field of electrochemistry of molten salts. Kobayashi et al. developed the two-dimensional finite element method (FEM) program for analyzing the secondary current distribution of the molten salt electrorefiner for the nuclear fuel reprocessing plant [1].

An integrated pyroelectrochemical method for recycling rare earths from spent hydrogen absorbing alloys, e.g., $LaNi_5$, has been developed. The procedure consists of the following three electrochemical processes, taking place in two electrolytic baths (Fig. 1 in [1]) [2 – 4]:

(i) Rare earths are anodically electrodissolved into a molten salt from spent hydrogen absorbing alloys in the first bath. The electrolyte is a LiCl-KCl eutectic melt (LiCl-KCl in 59 : 41 mol %) at 793 K. In the anode basket, the rare earths preferentially dissolve into the first bath. Electrodeposition $Me^{n+} + ne^- \rightarrow Me$ occurs on the cathode, where Me stands for lanthanum, cerium, neodymium, and lanthanum–cerium alloy. This method is interesting for obtaining an electrolyte rich in rare earths as the first step; thus the concentrations of rare earths at the cathode are a little less than those in the anode area. The quality of the rare earths electrodeposits is nevertheless acceptable under an appropriate electrodeposition condition.

(ii) In the electromigration cell (coexisting in the first bath), the rare earth cations are then further concentrated into the upper part of a column (one component of the electromigration cell) using the countercurrent electromigration method [5]. The enriched melt with rare earths is transferred to the second bath by suction.

(iii) The rare earths are finally cathodically electrodeposited in a metallic form in the second bath.

Then the same electrodeposition reaction of rare earths occurs on the cathode, where the electrolyte is much enriched with the selected rare earths compared with the first bath.

Hence, this method consists of two electrodeposition processes in the different baths, where there may be no significant difference in the electrodeposition conditions. So far, a preliminary experiment was conducted adopting a priori determined electrodeposition conditions (i.e. bath size and shape, electrolyte, electrolysis parameters, etc). Matsuura et al. reported that rare earths were successfully electrodeposited from spent hydrogen absorbing alloys using this trial electrodeposition condition, i.e. the bath being equipped with a special cathode [2, 4]. As a result, a few unresolved issues remained, mainly: less adherent and impure electrodeposits and a drop of electrodeposits.

As the special cathode, a ceramics dish possessing an edge attached to the cathode bottom, had been employed (hereafter abbreviated as 'cathode dish and edge', Fig. 1), which was suitable for preventing the loss due to drops of less adherent electrodeposits, i.e. dendrites and powdery electrodeposits. The morphology of the massive dendrites obtained should be closely related to the non-uniformity of the current density distribution [2, 4]. Despite the useful function of this accessory, the existence of the cathode dish might interfere with a smooth current flow into the cathode surface. Thus, some research into the effect of the cathode dish dimensions on the local current density distribution is required.

Dendrite or powdery electrodeposits have frequently been observed in molten salt electrodeposition, because the exchange current densities of metals are relatively higher than those in an aqueous solution [6]. The electrodeposits from a molten salt bath, electrolyte melt occlusion, might at first be suspected as impurity [7]. A non-uniform current density on the cathode surface will lead to a rough surface, resulting in dendrites, powdery electrodeposition, and an undulation of the electrodepositing surface. A dish connected with screw to the cathode has been expected to prevent the dispersion of dendrites and powdery electrodeposits into the melt. On the other hand, it may disturb the uniform current density. Thus, our research focuses on the optimization of the design of the dish attached to the cathode.

In actual electrodeposition operations, a low energy consumption and an effective utilization of raw materials are some of the important requirements, which might be accomplished by using a bath as small as possible. Under this constraint the optimization of the bath design will be carried out by the evaluation of the cathode current density distribution, varying the ratio of melt volume to electrode surface area.

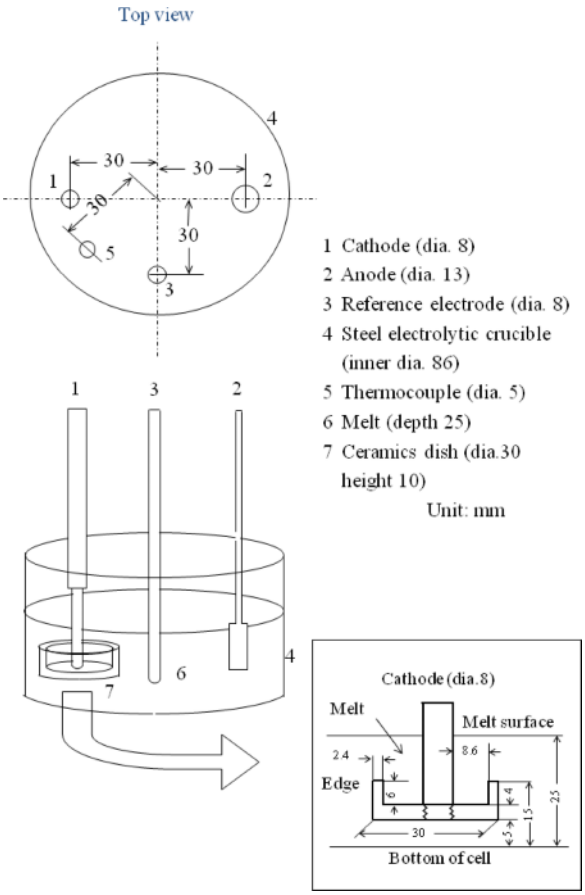

Fig. 1. Schematic diagram of the electrolytic bath and electrodes. Cathode: 8 mm in diameter, 16 mm in length, anode 13 mm in diameter, 15 mm in length. The inset shows the cathode dish with an edge (30 mm in outer diameter, 10 mm in height), which covers a volume of 8.6 mm diameter and 6 mm in depth around the lower part of the cathode.

In this study the best shape and size of the cathode dish is obtained by FEM, and a comparison is made between the results of this numerical simulation and those of the trial bath. Furthermore, the behaviour of the secondary current distribution of the cathode, the morphology of the electrodeposits, and the ratio of melt volume to electrode surface area of the baths are discussed using FEM.

Table 1. Input data for the calculations: average current densities, total currents, and time. The standard conditions are: 1000 A m^{-2}, 0.40 A, 7.2 s.

Physico-chemical properties of related materials at 600 °C		
Electrode	Electric conductance	$1.754 \cdot 10^7$ S/m
(La)	Density	6150 kg/m^3
	Electrochemical equivalent	$4.800 \cdot 10^{-7}$ g/C
	Current efficiency	1.000
Electrolyte	Electric conductance	246.9 S/m
Temperature		600 °C
Polarization curve	Multi point approximation from literature	
Current density	Average current density	1000 A m^{-2} as standard

	Average current densities [A m^{-2}]	Total current [A]	Time* [s]
1	100	0.040	72
2	200	0.080	36
3	500	0.200	14.4
4	1000	0.400	7.2
5	2000	0.800	3.6

* Total current and time are determined to maintain constant thickness.

2. Experimental

2.1. FEM Calculation

The full three-dimensional FEM simulation program (Electroplating Pilot System, Uyemura Co.) was used for the analyses of the secondary current distribution in the plating bath. It consists of FEMAP® (for FEM model formation and presentation, Structure Dynamics Research Co.) and EPPS® (for calculation and analysis, Uyemura Co.). This program is useful for obtaining quantitative time variations of composition, thickness, and morphology of electrodeposits. The flow of the calculation procedure is as follows:

1. input physico-chemical properties, dimension of the bath and accessories, and operating conditions;
2. set initial values and boundary conditions, including constant anode and cathode potentials and polarization curves;
3. make a geometrical model of the bath and accessory used for a preliminary experiment;
4. divide objects into three-dimensional polyhedron finite elements;
5. calculate secondary potential and current distributions;
6. check the convergence of the calculated data;
7. output potential and current contours.

As the boundary conditions, the electrode potentials were set on all electrode surface elements and so were the currents normal to the insulated walls of the bath. The thermocouple and the reference electrode were given conductance zero as von Neumann's condition (see also Tab. 1). The currents and potentials of all elements were determined by solving the Laplace equation. Since the sets of currents and potentials were not linear, the final values were determined by further calculations until the given convergence criteria were satisfied. In the convergence calculation, the average currents of the anode and the cathode were preliminarily obtained in order to adjust the sums of the currents for these electrode elements. Then the calculations were continued until the summed currents of both electrodes reached values close to the input data within the given allowance. Thus, this FEM calculation gave a simultaneous solution for i (the secondary current), the potentials E of individual meshed elements, and the time variations of the electrodeposits' thickness under the given boundary conditions (Tab. 1). As shown above, the average current densities of both electrodes were given as the experimental parameters, ranging from 100 to 2000 A m^{-2}. The FEM calculation procedure is described in detail elsewhere [8].

2.2. Electrodeposits Preliminary Obtained and Experimental Parameters for the Calculations

In the foregoing experiments electrodeposition [9] was performed adopting a priori determined standard conditions. However the shape of the electrodeposits was different between experiments and calculation. The experimental and calculated cross sectional profiles of the electrodeposits are shown in Figure 2, one

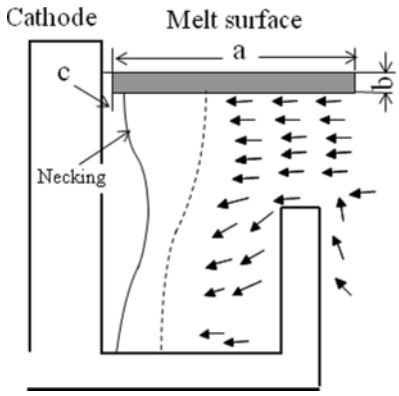

Fig. 2. Dimension of the artificially introduced floating mass possessing a high resistance (shaded area assumed on the basis of experiments; a = 22 mm, b = 2 mm, c = 1 mm) and the electrodeposit obtained experimentally (solid line) and calculated under standard conditions (dashed line). For clarification the distance of the solid and dashed lines from the cathode has been here chosen arbitrarily.

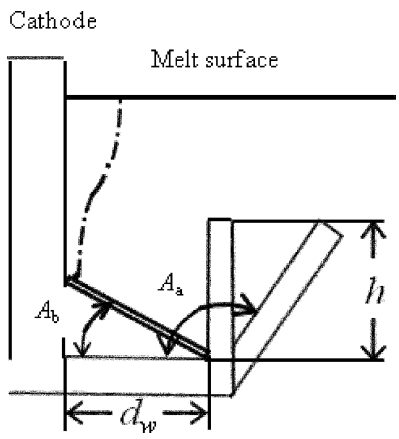

Fig. 3. Schematic drawing of the electrodeposition with the dish bottom at angle A_b (dashed line), the other experimental parameters are: dish bottom width d_w, edge height h, and edge angle A_a.

of these exhibits a necking, i.e. the phenomenon of local reduction of the diameters of the cylindrical cathode near the electrolyte surface. This necking is inconsistent with the profile calculated by FEM (dashed line), this implies an unidentified current flow disturbance. In the following section, this will be elucidated by FEM calculations including a resistive floating mass. Except for the necking, the assumed cathode form reproduced the experimentally obtained profile well.

The dimensions and arrangement of the electrolytic bath are shown in Figure 1. The inset in Figure 1 shows the dimension of the cathode together with the dish. The cathode dish should completely hold any detached electrodeposits; otherwise, they would disturb the current flow into the cathode surface. The electrolysis conditions are given in Table 1. In Figure 2, the current vectors show schematically the ionic current-streams flow. In Figure 3, the parameters for these FEM calculations were chosen as explained in the Discussion section. In this study, the differences between the maximum and minimum currents along the cathode were taken as a measure of the non-uniformity/uniformity of the secondary current density distribution.

3. Results and Discussion

3.1. Potential and Current Distributions of Cylindrical Cathode

Figure 4a shows the potential contour of the electrolyte surface and electrode circumference: the cathode (left hand side) and the anode (right hand side) under standard conditions. The potential (in V) is indicated by the color scale (scale bar shown on the right), referred to 0 V at the cathode surface. The shapes of both electrodes appear as empty cylinders embedded in the electrolyte. At the cathode, the equipotential lines are distorted, whereas the potential contours of a point charge (or a charged cylinder) are radially expanded as shown in Figure 4b. However, instead of electric force lines (defined to be orthogonal to equipotential lines), the current density distribution in a given volume element is considered in this paper (Appendix A).

The actual potential contours appear distorted; far from any radial symmetry (compare Figs. 4a and b). At the beginning of the calculations, the potential contours in Y-direction at both electrodes' circumferences (upper and lower directions in the figure) were almost symmetric with respect to the X-coordinate. This indicates that the existence of the reference electrode and the thermocouple do not disturb the potential contour. Taking the bath shape into account as well as the electrode arrangement with Y-symmetry (see Fig. 1 top view), the potential distribution also exhibits Y-symmetry. The potential contours of both electrodes in X-direction (for clarification shown as rectangles A and B in Fig. 4a) are denser than those shown as

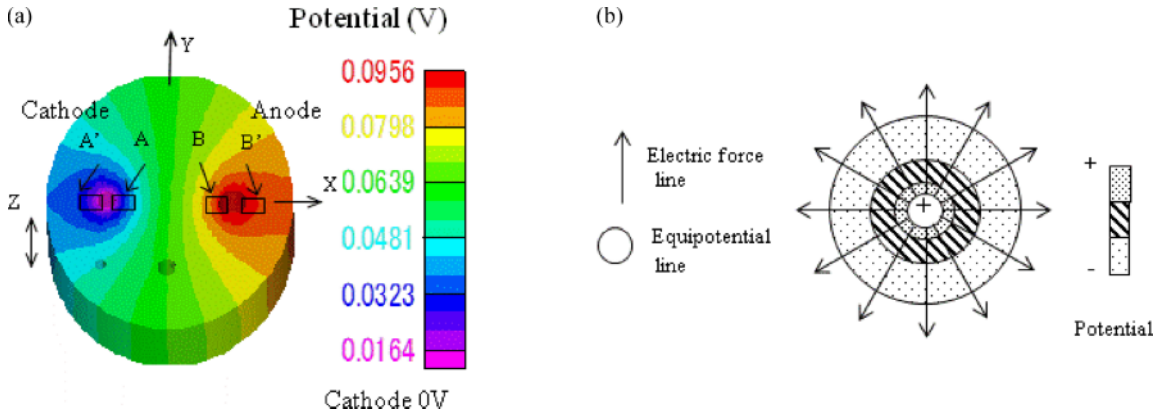

Fig. 4 (colour online). Potential contour plot of the electrolyte surface and electrode circumference under standard conditions (a), and schematic potential contour plot and electric force lines of a point charge (b).

A′ and B′. This means that the electric force lines in the vicinity of the cathode circumference are densest at the position nearest to the countered electrode (anode). Going from A to A′, the density of the potential contours gradually decreases. The same is valid in the anode case. Comparing the behaviour at the cathode with that at the anode at the nearest position to the countered electrode, that is A vs. B, the potential contours of the cathode are a little denser than those at the anode. The major part of the potential drops occurred around the cathode, and a further marked potential drop is concentrated in the area close to the countered electrode (along the X-coordinate), compared with a relatively small potential drop at back side, due to the interference of the crucible wall.

We have focused on the thickness distribution of the electrodeposit, i.e. the current density distribution along the Z-coordinate. Figure 5 shows the current density distribution (current contour, in $\mathrm{A\,m^{-2}}$) over the entire cathode surface at the standard current density $1000\ \mathrm{A\,m^{-2}}$, whereby the potential drops were converted to secondary current densities obeying Ohm's law (Appendix B). Similar to the potential contour, the calculated current densities at the front side exhibit higher values than those at the back, upper, and lower sides. As shown in Figure 5, the current densities vary gradually from a minimum to a maximum with increasing distance l (in mm) from the dish bottom. This current density distribution along the cathode reveals that the undesired irregular electrodeposits actually obtained are attributable to the non-uniformity of the current density along the cathode, described again below.

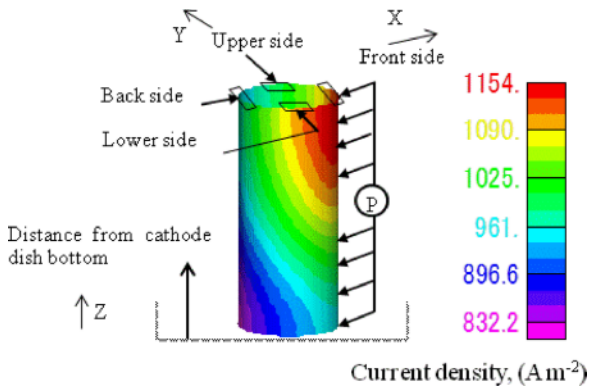

Fig. 5 (colour online). Current contour plot of the cylindrical cathode surface under standard conditions: average current density $1000\ \mathrm{A\,m^{-2}}$. P indicates the points where the current density distribution data are taken, called the front side. The front side (same as A in Fig. 4) is closest to the anode; the back side (same as A′ in Fig. 4) farthest to the anode and close to the wall; the upper and lower sides exhibit intermediate conditions between these two sides.

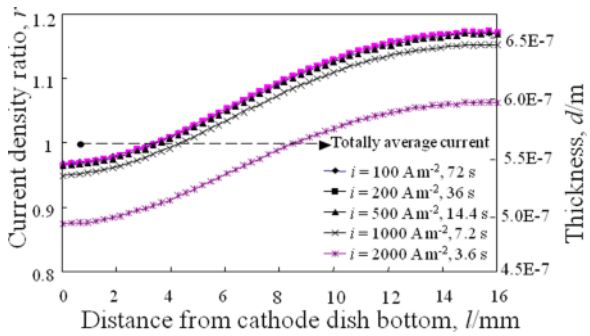

Fig. 6 (colour online). Current density ratio and thickness of the cathode surface at the front side vs. distance from the cathode dish bottom under standard conditions.

Figure 6 shows the current density ratios at the front side of the cathode vs. the distance from the cathode dish bottom for different average current densities. Here, the longitudinal axis unit is the ratio r of the local to the average current density. The data points are the nearest ones to the anode, i.e. at the front side, (P indicated in Fig. 5). The data at the other positions (upper, lower, and back sides) exhibit similar behaviour. The total ratio is set so that all positions around the cathode, at a given distance from the cathode dish bottom, should have values equal to unity. Thus, the average ratio at a given position, e.g. at front side, provides a measure of the extent to which the currents are distributed. To avoid the influence of the edge on the average ratio, these values, at the given position ranging from 6 up to 16 mm, were used for the evaluation. Since all curves in Figure 6 are regarded as the 'half wave' common pattern (see below Section 3.2) , the current density ratios at the front side decrease in the order of 100, 200, 500, and 1000 A m^{-2}, while that of 2000 A m^{-2} shifts to lower values, below the other ones. Because the current density ratios of the former are larger than one, a small amount of the current-streams turns around the cathode. Figure 6 reveals that except for a current density close to 2000 A m^{-2}, the amounts of the current-streams are nearly equal at the front, upper, lower, and back sides. It is said that current densities a little below 2000 A m^{-2} give an acceptable level and a radially even current distribution. As mentioned above, the effect of the imposed current density on the current density distribution is thus elucidated, although the relation between the current density ratios and the height of the cathode edge remains at a qualitative level.

Figure 6 also shows the thickness of the electrodeposits, referred to on the right hand axis, as a function of the average current densities. It seems that the thickness and the current density curves are identical. The thickness of electrodeposits is calculated, obeying Faraday's law, as follows. For a cathode element the thickness d of electrodeposit is calculated as

$$d = 10^{-3} itM/(\mathrm{nF}\rho)\,, \tag{1}$$

where i is the fixed current density, d is the thickness of the electrodeposit (m), t is time (s), M is the atomic weight (for alloys the average atomic weight is used), ρ is the density (kg m^{-3}), and nF is the electrochemical equivalent (C mol^{-1}).

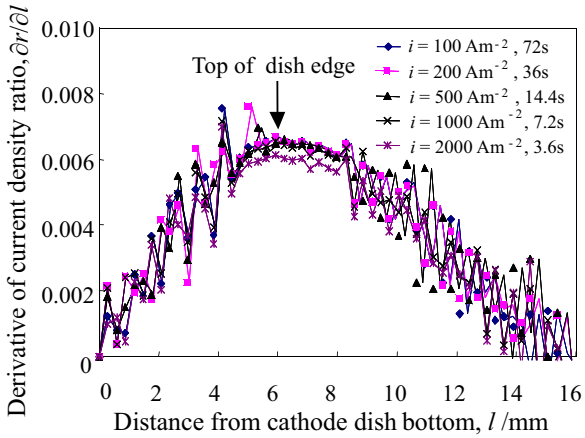

Fig. 7 (colour online). Derivative of the cathode current density $\partial r/\partial l$ vs. distance from the cathode dish bottom as a function of the average current densities.

Figure 7 shows the variation of the ratios of the current density vs. the distance (l/mm) from the bottom of the dish, that is $\partial r/\partial l$. As shown in Figure 7, the distance showing the maximum derivative value is coincident with that of the top position of the cathode dish edge (see also Fig. 3). It is apparent that the height h of the dish edge directly determines the dimension of the non-uniformity area. On the other hand, the condition $\partial r/\partial l = 0$ at $l = 0$ and 16 mm assures the uniformity of the electrodeposit thickness at the bottom and top of the cathode. The electrodeposition should hence, in theory, proceed smoothly at the bottom and top of the cathode.

Through the analysis of the current contours it was confirmed that the current density distribution in the radial direction was mostly attributable to the existence of the crucible wall, while that along the cathode (in the longitudinal direction) was determined by the influence of the cathode edge.

3.2. *Effect of Geometry of the Cathode Dish on the Current Density Distribution*

First, as an inhomogeneous electrodeposit might be attributed to some non-uniformity of the secondary current distribution, it is a key point to keep the current density homogeneous. With this in view, the dimensions and the shape of the cathode dish (Fig. 3) were varied while evaluating the current density distribution.

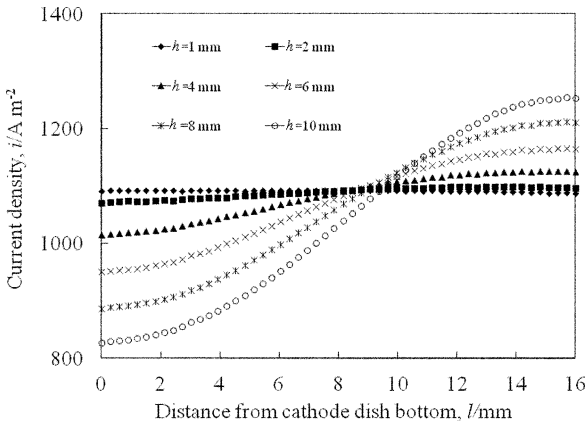

Fig. 8. Effect of the edge height h on the current density distribution curves.

The effects of the cathode edge height h, the dish bottom width d_w, the edge angle A_a, and the dish bottom angle A_b in Figure 3 on the current density distribution were examined, as exemplified in Figure 8 for the height h ranging from 1 up to 10 mm. Figure 8 shows that all current density distribution curves monotonically increase and reach a steady value asymptotically; these curves have been named the 'half wave pattern'. The current density distribution becomes more uniform with decreasing edge height. Considering this common behaviour, the differences between the maximum (max.) and minimum (min.) values of the current density are adopted as a directly obtainable measure of the non-uniformity of the current density distribution.

Figures 9a and b show plots of the differences between the maximum and minimum current densities vs. the various cathode dish parameter. From these two figures, it appears that the values of the differences increase with increasing edge height h, decreasing dish width d_w and angle A_a. As for A_b a minimum position appeared at 27°, however this would not be applicable. If we accept a slight increase of the value of the differences between the maximum and minimum current densities, 15° as A_b is recommended as the real design parameter. In Figures 9a and b, the dashed line indicates the value of the a priori determined parameters as the standard conditions (Tab. 1). However, the present results suggest a set of more adapted parameters, shown as dotted area with respect to the current density. As one parameter was varied independently, neglecting interactions with the others, the subsequent re-calculation of the initial parameters yielded $d = 12$ mm, $h = 4$ mm, $A_b = 120°$, leading to a lower value of the difference between the maximum and minimum current densities 145 A m^{-2} which is an improvement of the current density distribution compared with the value of ca. 215 A m^{-2} using a priori determined value.

3.3. Effect of the Bath Size

The requisite of a small bath size is important not only because of economic considerations but also for the reduction of secondary disposable wastage. In practice, the bath size has been determined by empirical formulae and experience. The ratio of electrolyte volume to electrode surface area is an important pa-

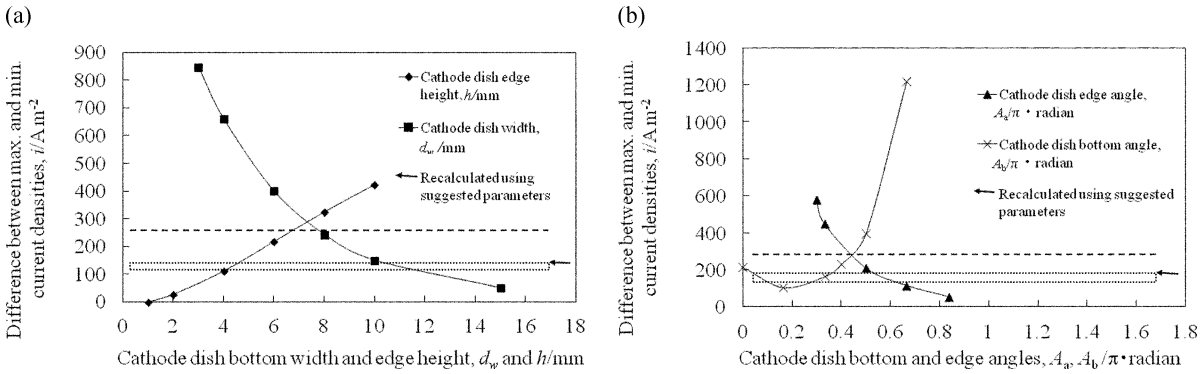

Fig. 9. Effect of various cathode dish parameters on the differences between the maximum and minimum current densities. The dashed line and the dotted area indicate the standard conditions and the optimal cathode dish design parameters: $d = 12$ mm, $h = 4$ mm, $A_a = 120°$, respectively.

	u	v	w		No. of data	Reference No. in Fig. 10
Cylinder	20	30	46–59		5	Cylinder 1
	10.75–26.15	10.75–26.15	27.75-43.17		5	Cylinder 2
	u	v	p	q		
Box	20	30	90	31–60	6	Box 3
	6.75–20	15.75–30	45.5–74	31	6	Box 4
	20	30	90–110	31	6	Box 5

Table 2. Parameters for both types of bath for calculation. u, v, w, p, q are indicated in Figure 10. The unit is mm.

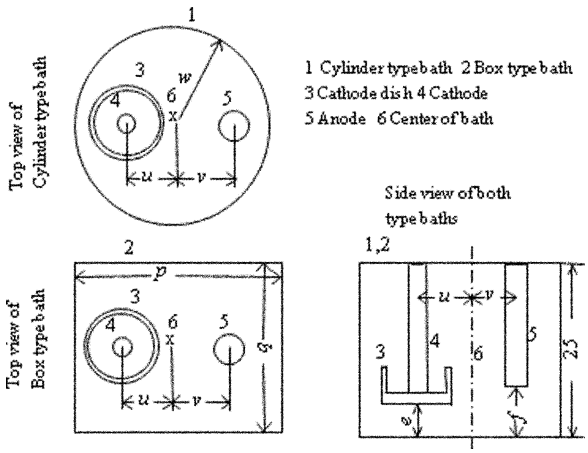

Fig. 10. Cylinder and box type baths for effective bath size control. The geometry of the electrodes and the melt level are kept constant at the standard condition. The unit is in mm.

rameter for the electrode and bath design. In Figure 10, these two kinds of baths (cylinder and box types) are drawn for the parameters w, u, and v set for a fixed separation between both electrodes (u and v), and for a variable separation. For a more flexible bath size control another box type bath is drawn, where p and q are independently varied with the fixed and variable separations (Tab. 2). Through a multiple parameter survey it was noticed that reducing the bath size at a constant electrode surface area is equivalent to a reduction of the ratio of volume to surface area (or electrolyte volume). Figure 11 shows plots of the differences between the maximum and minimum current densities vs. the electrolyte volume: the differences decrease with increasing electrolyte volume. The differences between the maximum and minimum current densities are a unique function of the electrolyte volume except the Box 5. In Figure 11, under standard conditions, a rather high electrolyte volume and a difference of ca. 215 A m^{-2} (indicated by an arrow in the figure) are found. If the electrolyte volume is reduced to ca. 50 cm^3, this reduction by about one-fifth is accompanied by a slight increase of 60 A m^{-2} in the current density. Since the costs involved for the volume change are small compared with the ones for an improvement through a cathode dish adjustment, a smaller bath

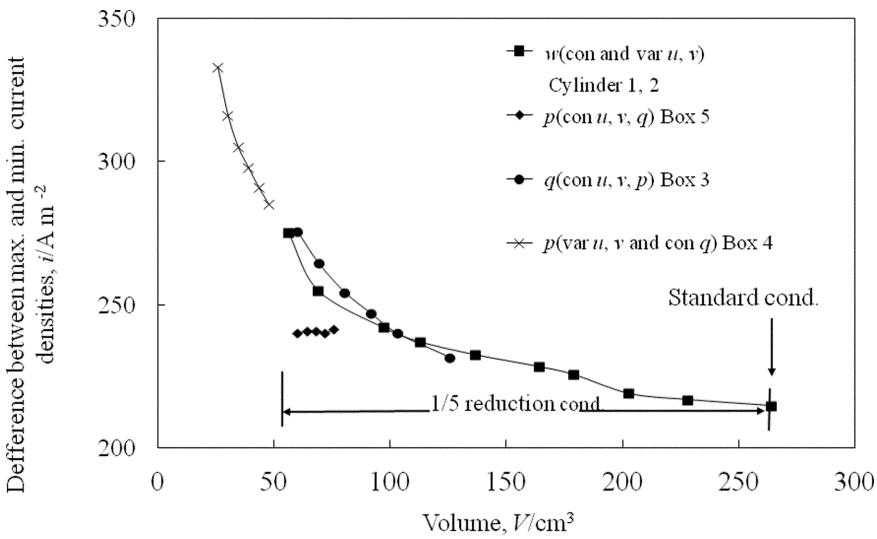

Fig. 11. Effect of the electrolyte volume on the differences between the maximum and minimum current densities with various bath parameters. Each line shows the variation of the main parameter while the others are kept constant. The details are tabulated in Table 2.

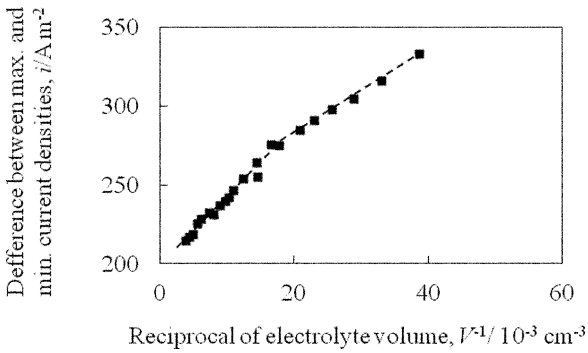

Fig. 12. Effect of the reciprocal of electrolyte volume on the differences between the maximum and minimum current densities with various bath parameters.

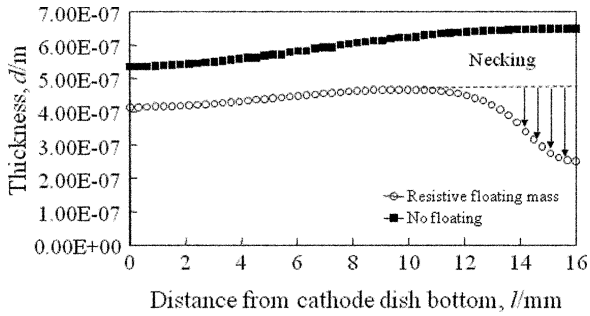

Fig. 13. Thickness of the electrodeposit, calculated using the standard conditions and with the resistive floating mass shown in Figure 2. The dimension of the artificially introduced floating mass with a high resistance: a = 22 mm, b = 2 mm, c = 1 mm.

may be recommended. Comparing the Cylinder 1 and Cylinder 2 cases (denoted in Tab. 2), a reduction of w (cylinder radius) gives an increase of the differences, independent of values of u and v. Comparing furthermore Box 3 and 5 one sees that a reduction of q (the longitudinal wall distance) at constant u, v, and p gives a similar increase of the differences while a reduction of p (lateral wall distance) gives a negligible effect. This difference between the two box cases is explained as follows: in a box type bath the current flow is mostly influenced by a shrinkage of the gap between the crucible wall and the cathode edge (corresponding to q), not by a narrowed back side space (corresponding to p). For Box 4, the reduction of u and v deteriorates the differences considerably, even if $q = 31$ mm and p ranging 45.7 to 74 mm are assumed to increase the differences.

The differences vary in the range of ca. 0 to 1200 A m^{-2} with varying dimensions of the cathode (see Fig. 9), while these differences change with varying bath size (or electrolyte volume) between 210 to 340 A m^{-2} (see Fig. 11). These results should lead to a more effective bath design taking into account both economical and environmental aspects.

Figure 12 shows that the differences are replotted against the reciprocal of the electrolyte volume. This plot exhibits a straight line with different slopes, which can be expressed as

$$\begin{aligned}\text{Diff.}\,(\mathrm{A\,m^{-2}}) &= \\ &4.58\cdot(\text{reciprocal of volume in cm}^{-3}) \\ &\cdot 10^3 + 200 \quad \text{at 0–16.36(in } \cdot 10^3\text{cm}^{-3})\,,\end{aligned} \tag{2}$$

$$\begin{aligned}\text{Diff.}\,(\mathrm{A\,m^{-2}}) &= \\ &2.64\cdot(\text{reciprocal of volume in cm}^{-3}) \\ &\cdot 10^3 + 275 \quad \text{at 16.36–40(in } \cdot 10^3\text{cm}^{-3})\,.\end{aligned} \tag{3}$$

The relation between the differences and the electrolyte volume provides in practice significant information for estimating the bath dimensions within a given allowable difference.

3.4. Morphology of an Electrodeposit Affected by Highly Resistive Surface Floating

Figure 13 shows the thickness variation of the electrodeposit under standard conditions and with a highly resistive surface floating mass (dimensions shown in Fig. 2), where the material of the floating mass is estimated to be Li_2O or lanthanum oxichloride. The latter floating mass is the one expected by the authors, its resistance, however, is unknown; the value of La_2O_3 (electric resistance $1.0\cdot 10^4$ Ωm [10]) is adopted in this calculation. As is seen in Figure 13, the thickness of the electrodeposit anomaly goes down while approaching the melt surface. Figure 2 shows the electrodeposit profile obtained experimentally under similar experimental conditions. The calculated electrodeposit profile agrees qualitatively with the experimental one, which indicates that this sudden deviation of the current density (or thickness of electrodeposit) is attributable to the artificially located obstacle. In former experimental runs, a surface floating mass was observed in the case of $LaNi_5$ [4], which was used also as the anode.

Further parameter fitting analysis is required to identify the material of an object, accompanied with the accurate analyses of the surface floating mass.

4. Conclusion

FEM calculations were used for the optimization of a molten salt electrolytic bath and its cathode accessories for rare earth metal recovery. One of the goals was to obtain a uniform current distribution. It was shown that optimized electrolysis conditions can be satisfactorily predicted from the analysis of the secondary current distribution. If the bath size needs to be changed, an appropriate bath structure can be obtained as a function of the ratio of the electrolyte volume to the surface area. The following results, including the desirable design parameters, were obtained in this work:

i. The desirable level for the average current density, a little less than 2000 $\mathrm{A\,m^{-2}}$, is compatible with a radially symmetric current density distribution.
ii. The current density distribution along the cathode can be determined by varying the shapes of the cathode dish.
iii. The parameter survey showed that the optimized cathode dish ($h = 4$ mm, $d_w = 12$ mm, and angle $A_a = 120°$, see Figs. 3 and 9) gives an improvement for the current density distribution.
iv. Economic considerations lead us to evaluate the dimensions of smaller baths. An empirical relation between the differences of maximum and minimum current densities and the reciprocal of the electrolyte volume was obtained.
v. It was elucidated that 'necking' appearing in the electrodeposit profile can be attributed to the existence of a resistive floating mass.

Appendix A

From Faraday's definition, bundled electric force lines are generated from positive charges (or a charged cylinder) to negative ones. The local current density in a certain area shown, by vectors, is defined as the mean orientations of the tangent of the electric force lines and the magnitude corresponding to those densities. Therefore, if an obstacle interferes, the electric force lines stream around it, e.g., for an artificial window set, there exists a bunch of electric force lines, the density of which exhibits a high value. In this way the local density of the electric force lines between the anode and cathode surfaces shows high and low regions. Accordingly, the magnitude of the local current density makes the distributions from the principle.

Alternatively, in this calculation the magnitude of the local current density is directly converted by (B.1) below. It is proportional to the electric field, irrespective of the behaviour of the electric force lines (Appendix B). For the sake of clarity, the electric force lines are related with the local current density: an area with dense equipotential lines (or closer potential contours), and a strong electric field. The dense electric force lines are related accordingly to a high local current density, the direction of which points along the steepest slope of equipotential lines. The reverse is valid in the areas with thin equipotential lines (or wider potential contours).

Appendix B

The secondary potential $\varphi(k)$ at each element k is calculated and then the secondary current density in each element $j(k)$ is determined by

$$j(k) = -\kappa\Delta\varphi(k)\,, \tag{B.1}$$

where κ is the electric conductance of the melt, φ is the potential, and $\Delta\varphi$ is the electric field.

Acknowledgements

The authors would like to thank Mr. Katsuhiko Ohara at Uyemura Co. for creating the FEM computer code for the floating mass. This work is supported by the Industrial Technology Research Grant Program from the New Energy and Industrial Technology Development Organization (NEDO) of Japan (00B62009C).

[1] T. Kobayashi, R. Fujita, M. Fujie, and T. Koyama, J. Nucl. Sci. Technol. **32**, 653 (1995).
[2] H. Matsuura, The Report of Industrial Technology Research Grant Program, No. 00B62009C, the New Energy and Industrial Technology Development Organization (NEDO), Kawasaki, Japan (in Japanese).
[3] R. Fujita and Y. Akai, J. Alloys. Compd. **271–273**, 563 (1998).

[4] H. Matsuura, H. Numata, R. Fujita, and H. Akatsuka, J. Phys. Chem. Solids **66**, 439 (2005).
[5] A. Klemm, Z. Naturforsch. **1**, 252 (1946).
[6] S. Haruyama, H. Numata, and A. Nishikata, Proc. of 1st Int. Symp. on Molten Salt Chem. and Tech., Kyoto, Molten Salt Commun., Electrochem. Soc. of Japan, pp. 153 – 156 (1983).
[7] Private communication with M. Ginatta's group in Italy (1992).
[8] K. Ohara, Hyoumen Gijyutsu **50**, 416 (1999) (in Japanese).
[9] H. Numata, H. Matsuura, R. Fujita, and H. Akatsuka, 71st Annual Meeting Electrochem. Soc. Japan, Yokohama, Ab., p. 61 (2004) (in Jananese).
[10] U. Croatto and A. Mayer, Grazz. Chim. Ital. (Roma) **73**, 199 (1943).